materials **MDPI**

Article

The Influence of Annealing on the Structural and Soft Magnetic Properties of $(Fe_{0.4}Co_{0.6})_{79}Nb_3B_{18}$ Nanocrystalline Alloys

Man Zhu *, Yang Fa, Lijuan Yao, Peng Tao, Zengyun Jian and Fang'e Chang

School of Materials Science and Chemical Engineering, Xi'an Technological University, Xi'an 710021, China; fayang2025@163.com (Y.F.); ylj8453@126.com (L.Y.); 18762794998@126.com (P.T.); jianzengyun@xatu.edu.cn (Z.J.); cfe.ch@163.com (F.C.)

* Correspondence: zhuman0428@126.com; Tel.: +86-029-8617-3324

check for updates

Abstract: The soft magnetic properties of Fe-based nanocrystalline alloys are determined by their grain size. In the present article, the $(Fe_{0.4}Co_{0.6})_{79}Nb_3B_{18}$ nanocrystalline alloys have been successfully prepared by isothermal annealing. The variation of soft magnetic properties as a function of annealing temperature and incubation time is investigated in detail. Two distinct crystallization behaviors were found for the $(Fe_{0.4}Co_{0.6})_{79}Nb_3B_{18}$ alloys. The initial nanocrystallization products comprise a mixture of α-Fe(Co), Fe_2B, and $Fe_{23}B_6$-type crystalline metastable phases, and the final crystallization products are composed of α-Fe(Co), Fe_2B, and Fe_3B crystalline phases. The grain size decreases first and then increases with the increasing annealing temperature in the range of 764–1151 K, and a fine grain size with mean grain size of 12.7 nm can be achieved for alloys annealed at 880 K. As the annealing temperature increases from 764 K to 1151 K, the saturation magnetization increases first and then decreases without a significant increase of the coercivity. The alloys annealed at 880 K exhibit the optimized soft magnetic properties with high M_s of 145 emu g^{-1} and low H_c of 0.04 Oe.

Keywords: Fe-based nanocrystalline alloys; isothermal annealing; grain size; soft magnetic properties

1. Introduction

In 1988, Yoshizawa et al. [1] developed a new series of FeCuNbSiB nanocrystalline alloys with excellent magnetic properties. In 2013, Rizal et al. [2] artificially produced Fe-Co alloys with record high saturation magnetization (M_s > 240 emu/g). This group claimed that the increase of M_s is correlated with the increase of the lattice constant of the alloy. Thus, these Fe-based soft magnetic alloys have received great attention in the materials field [3–5]. The Fe-based nanocrystalline alloys with high performance have been served as the magnetic cores, sensors, and transformers in electrical industrial fields, and they are potential candidates to replace traditional soft magnetic alloys, such as silicon steel and ferrite. Generally speaking, metallic glass is in a thermodynamically metastable state. Upon heating, it would transform into a stable state by a crystallization process to form amorphous/nanocrystalline alloys. The soft magnetic properties in the Fe-based nanocrystalline alloys are determined by the type and grain size of the nano-scale precipitates. Nowadays, annealing crystallization is one of the key methods used to prepare Fe-based nanocrystalline alloys [6–10]. Therefore, it is of theoretical significance and engineering application value to explore the relationship between their magnetic properties and annealing process. Generally speaking, the grain size increases with increasing annealing temperature [11–13]. However, according to recent studies, as the annealing temperature increases, the grain size increases first, then decreases, and increases again in the Fe-based nanocrystalline alloys [14,15]. Xue et al. [14] pointed out that the grain size reaches the minimum

value for the $Fe_{83}Nb_2B_{14}Cu_1$ alloys annealed at 813 K, while their saturation magnetization increases steadily from 1.4 T to 1.7 T with the increase of annealing temperature. Li et al. [15] pointed out that the $Fe_{73.37}Cu_{0.92}Nb_{2.9}Si_{13.56}B_{9.24}$ nanocrystalline alloys with the finest grain size exhibited optimized magnetic properties. However, the experiments carried out by Jiang et al. [16] indicated that the grain size in the $Fe_{73.5}Cu_1Nb_3Si_{13.5}B_9$ nanocrystalline alloys decreases slightly, and then increases with increasing annealing temperature, and the anomalous grain growth is ascribed to the different nucleation and volume diffusion rates at varied annealing temperatures. The variation of grain size as a function of annealing during the annealing process remains unclear, and it is quite difficult to determine the optimized annealing process for alloys with excellent soft magnetic properties. It is accepted that fine and well-distributed nanoscale precipitates within the amorphous matrix are of benefit to enhance the magnetic properties. Thus, it is of great importance to study the relationship between magnetic properties and the annealing process.

In this article, the aim is to explore the relationship between grain size and annealing temperature in the $(Fe_{0.4}Co_{0.6})_{79}Nb_3B_{18}$ alloys. In addition, the soft magnetic properties as a function of the kinds and size of the precipitates are also studied, which can provide theoretical guidance for the development of Fe-based nanocrystalline alloys with excellent soft magnetic properties.

2. Materials and Methods

Master alloy ingots with nominal composition of $(Fe_{0.4}Co_{0.6})_{79}Nb_3B_{18}$ were prepared by induction melting (SPG-40B high frequency induction heating equipment, Shenzhen, China) the mixture of pure Co (99.98 wt%), Fe (99.8 wt%), Fe-60 wt% Nb and Fe-17.5 wt% B master alloy. Then, the amorphous ribbons were prepared by melt-spinning method under high vacuum single-roller spinning equipment. During this process, the linear velocity and ejection pressure are 40 m/s and 20 kPa, respectively. The resulting ribbons have a thickness of 20–30 μm. Then, the isothermal annealing experiment was performed for the glassy ribbons sealed into quartz tubes under vacuum condition (4×10^{-3} Pa) in a resistance furnace. The annealing temperature (T_a) was set as 764 K, 800 K, 880 K, 974 K, and 1151 K.

Phase constitution was identified by X-ray diffractometer (XRD; Bruker D8 advance, Bruker AXS GmbH, Karlsruhe, Germany) with Cu Kα as a radiation (λ = 0.154056 nm) in steps of 0.02° in the 2θ = 30–120°. Thermal behaviors of the glassy ribbons were studied using differential scanning calorimetry (DSC; Mettler–Toledo TGA/DSC1, Mettler-Toledo International Inc., Zurich, Switzerland) at a continuous heating rate of 40 K min^{-1}. Room-temperature magnetic hysteresis loops were measured using a vibrating sample magnetometer (VSM; Lake Shore 7410, Lake Shore Cryotronics, Columbus, OH, USA) under an applied magnetic field of 10,000 Oe.

3. Results and Discussion

3.1. Structure Identification and Thermal Properties in the As-Quenched $(Fe_{0.4}Co_{0.6})_{79}Nb_3B_{18}$ Alloys

Figure 1a shows the XRD pattern taken from the as-quenched $(Fe_{0.4}Co_{0.6})_{79}Nb_3B_{18}$ alloys. Only a wide diffraction peak in the 2θ region of 35–55° can be observed, and no sharp Bragg diffraction peaks corresponding to the crystalline phases are detected. This is the typical characteristic of amorphous alloys, indicating that a fully amorphous structure is obtained in the $(Fe_{0.4}Co_{0.6})_{79}Nb_3B_{18}$ alloys.

Figure 1b displays the DSC heating trace of the as-quenched $(Fe_{0.4}Co_{0.6})_{79}Nb_3B_{18}$ alloys with a constant heating rate of 40 K min^{-1}. During the heating process, it undergoes a glass transition event followed by a supercooled liquid region, and then two-stage crystallization events are observed. The value of glass transition temperature (T_g) is equal to 732 K, and the values of first crystallization onset temperature (T_{x1}) and second crystallization onset temperature (T_{x2}) are equal to 786 K and 887 K, respectively. The supercooled liquid region $\Delta T_x = T_{x1} - T_g$, is estimated to be 54 K. In the high-temperature region, there are two endothermic peaks. The values of solidus temperature (T_m) and liquidus temperature (T_l) are 1219 K and 1444 K, respectively. The parameter T_{rg} ($=T_g/T_l$) is calculated to be 0.507. The results suggest that present $(Fe_{0.4}Co_{0.6})_{79}Nb_3B_{18}$ alloys possess high glass forming

ability (GFA). The temperature intervals ΔT_N between two crystalline peaks, defined as $T_{x2} - T_{x1}$, reach 101 K. It is reported that large ΔT_N is of benefit to the fabrication of amorphous/nanocrystalline alloys by precisely controlling the annealing process.
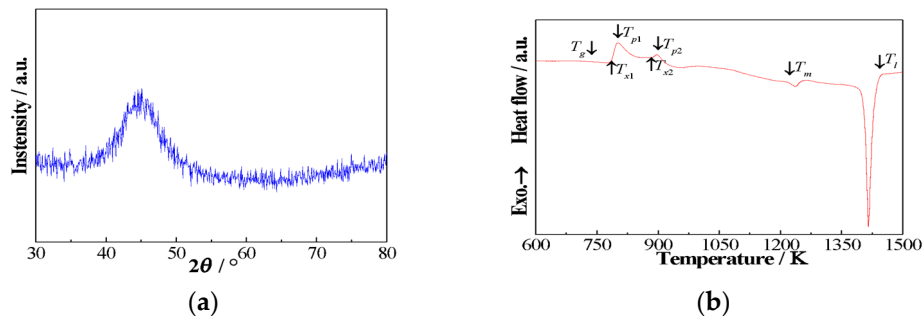

Figure 1. XRD pattern (**a**) and DSC heating curve (**b**) of the as-quenched $(Fe_{0.4}Co_{0.6})_{79}Nb_3B_{18}$ alloys.

3.2. Structural Evolution in the Annealed $(Fe_{0.4}Co_{0.6})_{79}Nb_3B_{18}$ Alloys

The $(Fe_{0.4}Co_{0.6})_{79}Nb_3B_{18}$ alloys were isothermally annealed at a temperature of T_a = 764 K, which is near T_{x1} between T_g and T_{x1}. Figure 2 exhibits the XRD patterns of the $(Fe_{0.4}Co_{0.6})_{79}Nb_3B_{18}$ alloys annealed at 764 K for different incubation times. The crystallization products are composed of α-Fe(Co), Fe_2B, and $Fe_{23}B_6$ phases for alloys annealed for 60 s. As the incubation time increases from 90 s to 900 s, the crystallization products still remain unchanged. The results indicate that increasing incubation time cannot change the crystallization process.
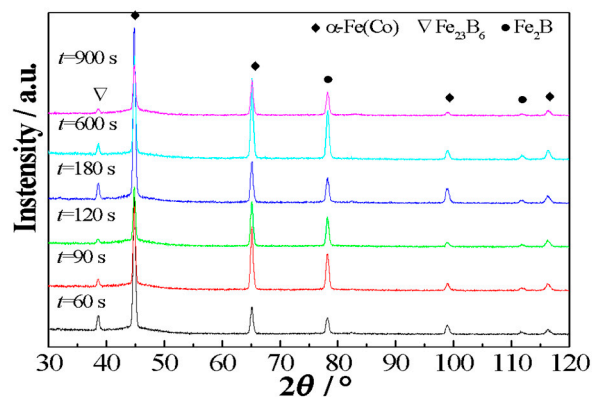

Figure 2. XRD patterns of the $(Fe_{0.4}Co_{0.6})_{79}Nb_3B_{18}$ alloys annealed at 764 K for varied times.

Figure 3 displays the XRD patterns of the $(Fe_{0.4}Co_{0.6})_{79}Nb_3B_{18}$ alloys annealed at 764 K, 800 K, 880 K, 974 K, and 1151 K for 90 s, respectively. For alloys annealed at 764 K, the crystallization products consist of a mixture of α-Fe(Co), $Fe_{23}B_6$, and Fe_2B phases. The formation of a metastable $Fe_{23}B_6$ phase was previously reported in the FeNbB ternary alloys [3,17–19]. It has an *fcc* structure with a lattice constant of a = 1.076 nm. In this structure, the cubo-octahedra and the cubes formed by metal atoms are symmetrically connected with metalloid atoms. Thus, it would prevent long-range ordered diffusion during the solidification process, which favors the enhancement of GFA. For the alloys annealed at 800 K and 880 K, which range from T_{x1} to T_{x2}, the crystallization products remain unchanged, and they are composed of α-Fe(Co), $Fe_{23}B_6$, and Fe_2B phases. Because of the relatively short incubation time, the $Fe_{23}B_6$ phase is not completely decomposed. Thus, the existence of the metastable $Fe_{23}B_6$ phase still can be detected in the XRD patterns. Although the crystallization products remain unchanged, the corresponding width and intensity of the Bragg diffraction peaks change. This phenomenon suggests that the α-Fe(Co), $Fe_{23}B_6$, and Fe_2B phases undergo grain growth processes, and their volume fraction increases. When the annealing temperature is larger than T_{p2}, the crystallization products consist of

α-Fe(Co), Fe$_2$B, and Fe$_3$B phases for alloys annealed at 974 K. The existence of Fe$_2$B and Fe$_3$B phases is attributed to the decomposition of the metastable Fe$_{23}$B$_6$ phase. As the annealing temperature is further increased to 1151 K, the crystallization products remain composed of α-Fe(Co), Fe$_2$B, and Fe$_3$B phases. The amount of relative diffraction peaks of Fe$_2$B and Fe$_3$B phases is increased, suggesting that the volume fractions of Fe$_2$B and Fe$_3$B phases are enhanced. Therefore, the crystallization processes in the (Fe$_{0.4}$Co$_{0.6}$)$_{79}$Nb$_3$B$_{18}$ alloys can be expressed as:

$$\text{Amorphous} \rightarrow \text{Amorphous} + \alpha\text{-Fe(Co)} + \text{Fe}_{23}\text{B}_6 + \text{Fe}_2\text{B} \rightarrow \alpha\text{-Fe(Co)} + \text{Fe}_2\text{B} + \text{Fe}_3\text{B}$$
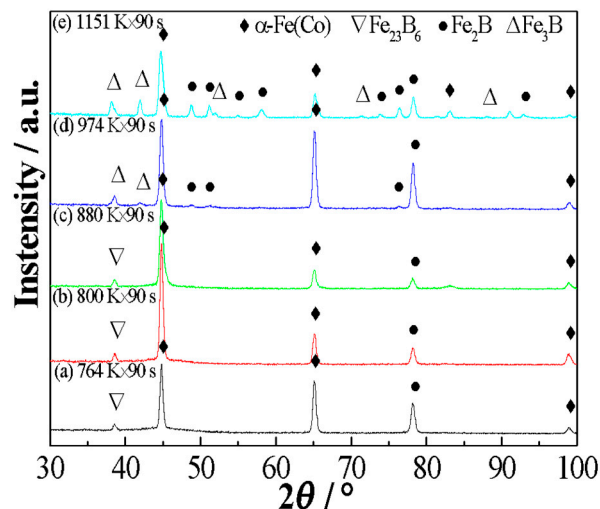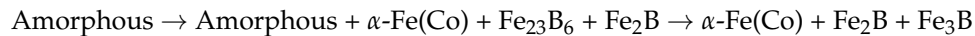

Figure 3. Structural evolution of the (Fe$_{0.4}$Co$_{0.6}$)$_{79}$Nb$_3$B$_{18}$ alloys annealed at different temperatures for 90 s.

The crystallinity refers to the degree of crystallization of amorphous alloys under different heat treatment processes. The crystallinity, X_c, can be expressed as,

$$X_c = \frac{W_c}{W_c + W_A},\tag{1}$$

where W_c and W_A represent the mass fraction of the crystalline phase and amorphous phase, respectively.

Figure 4 shows the relationship between crystallinity X_c and annealing temperature T_a. The value of X_c is equal to 68.69% for alloys annealed at 764 K. With the increase of the annealing temperature, the crystallinity increases steadily. As the annealing temperature is further increased to 1151 K, the value of X_c becomes 98.88%.
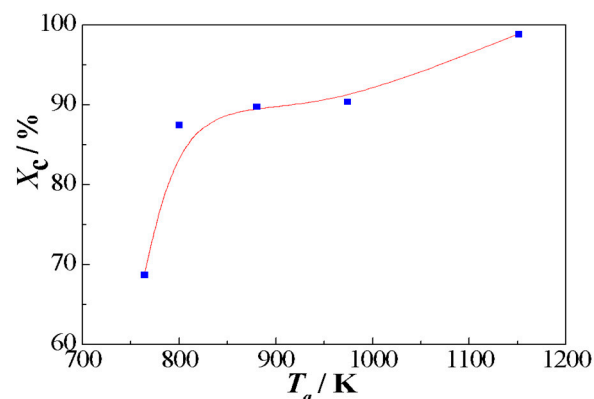

Figure 4. Variation of crystallinity as a function of annealing temperature for the (Fe$_{0.4}$Co$_{0.6}$)$_{79}$Nb$_3$B$_{18}$ alloys.

3.3. Variation of Grain Size and Annealing Temperature

According to the Scherrer Equation [6], the mean grain size (*D*) of the crystallite can be expressed as:

$$D = \frac{k\lambda}{\beta \cos\theta}, \tag{2}$$

where λ is wavelength, θ is half the diffraction angle, β is full-width at half-maximum (FWHM) of the diffraction peak, and k is the constant (k = 0.89).

The mean grain size (*D*) as a function of annealing temperature is plotted in Figure 5, and the corresponding DSC curve is also given. With the increase of the annealing temperature within the range 764–1151 K, the mean grain size decreases steadily and then increases. In other words, the grain size has obvious valley value with the change of the annealing temperature. The mean grain size (*D*) is equal to 18.2 nm and 17.7 nm for alloys annealed at 764 K and 1151 K, respectively. It reaches the minimum value of 12.7 nm for alloys annealed at 880 K.
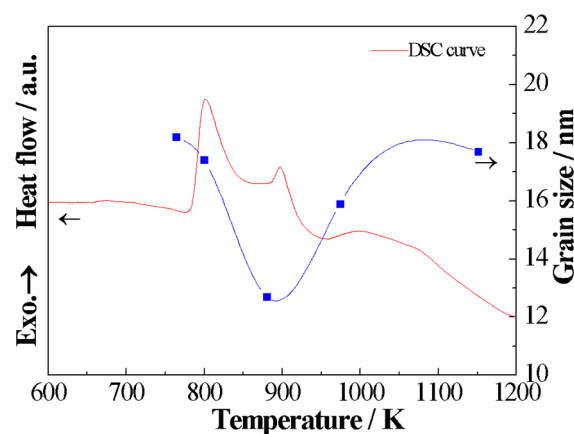

Figure 5. The relationship between mean grain size and annealing temperature for the $(Fe_{0.4}Co_{0.6})_{79}Nb_3B_{18}$ alloys.

The relationship between mean grain size and annealing temperature is in accordance with that predicted by theoretical analysis [20,21]. In other words, when the annealing temperature is equal to $0.6\, T_m$, the mean grain size reaches the minimum value. It is directly related to the combined effect of a high nucleation rate and low grain growth rate. The crystallization process includes nucleation and grain growth processes. The nucleation rate $I(T_a)$ and grain growth rate $U(T_a)$ can be expressed as [20,22]:

$$I(T_a) = I_0 \exp\left(-\frac{\lambda \Delta S_m^f}{R\tau^2(1-\tau)^3}\right) \exp\left(-\frac{\Delta E_n}{RT_a}\right), \tag{3}$$

$$U(T_a) = U_0 \left[1 - \exp\left(-\frac{\Delta S_m^f \tau}{R(1-\tau)}\right)\right] \exp\left(-\frac{\Delta E_g}{RT_a}\right), \tag{4}$$

where ΔS_m^f is melting entropy, τ ($=1 - T_a/T_m$) the undercooling, R the gas constant, ΔE_n the activation energy of nucleation, ΔE_g the activation energy of diffusion, T_a the annealing temperature, T_m the melting temperature, and I_0, U_0, and λ are the constants.

It can be found that the nucleation rate $I(T_a)$ is determined by T_a and ΔE_n, and grain growth rate $U(T_a)$ is associated with T_a and ΔE_g. The relationship between the nucleation rate and grain growth rate and annealing temperature is schematically plotted in Figure 6 [6], and T_x and T_m represent the first crystalline temperature and melting point, respectively. With the increase of T_a, $I(T_a)$ and $U(T_a)$ increase first and then decrease. As the temperature increases from the first crystalline temperature to the temperature of the extreme value of the nucleation rate, the nucleation rate increases faster than the grain growth rate, and it reaches the extreme value quickly. Previous theoretical research confirmed

that, when the annealing temperature is equal to approximately $0.6T_m$, a high nucleation rate and low grain growth rate can be achieved. Thus, it is reasonable to believe that the nanocrystalline alloys with fine grain sizes can be obtained for alloys annealed in the vicinity of $0.6T_m$.
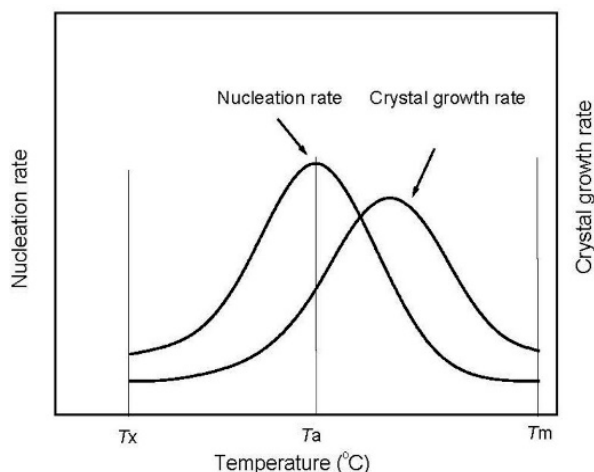

Figure 6. Schematic diagram showing the plots of nucleation rate and grain growth rate as a function of annealing temperature.

3.4. Soft Magnetic Properties

Figure 7a displays the room-temperature magnetization hysteresis curves (*M–H*) of the $(Fe_{0.4}Co_{0.6})_{79}Nb_3B_{18}$ alloys annealed at 764 K for 60–900 s, and the inset shows the enlarged image of the *M–H* curves. As can be seen from Figure 7a, the annealed alloys exhibit obvious soft magnetic properties without a significant increase of the coercivity. Figure 7b exhibits the relationship between saturation magnetization (M_s) and coercivity (H_c) and incubation time (t) in the $(Fe_{0.4}Co_{0.6})_{79}Nb_3B_{18}$ alloys. The M_s value is equal to 113 emu g^{-1} for the as-quenched $(Fe_{0.4}Co_{0.6})_{79}Nb_3B_{18}$ alloys. Annealing for 60 s does not result in a significant change in M_s. As the incubation time further increases, the M_s value increases steadily. When the incubation time is equal to 900 s, the M_s value reaches the maximum value of 132 emu g^{-1}. The increase of the M_s value is mainly determined by the grain size and volume fraction of the nano-scale precipitates. However, as the incubation time increases, the H_c value decreases slightly and then increases, and reaches 0.56 Oe for alloys annealed for 900 s. Short-time annealing benefits the reduction of internal stress, resulting in a slight decrease of M_s. However, further annealing leads to an increase in grain size, resulting in high M_s.
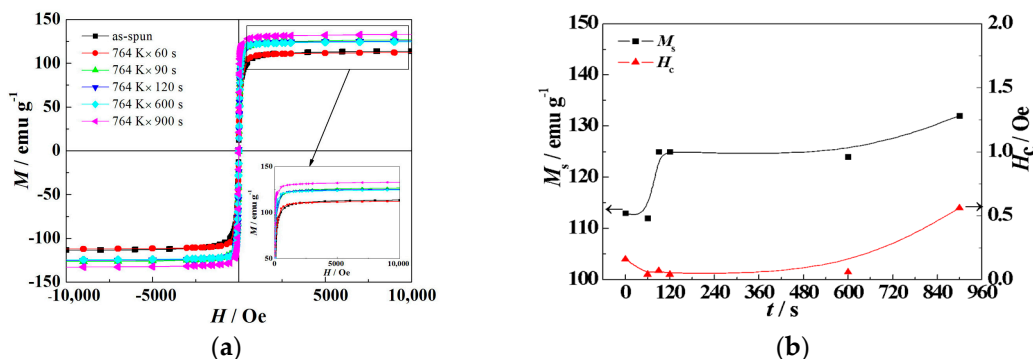

Figure 7. Magnetization hysteresis curves taken from the $(Fe_{0.4}Co_{0.6})_{79}Nb_3B_{18}$ alloys annealed at 764 K (**a**) and the variation of M_s and H_c as a function of incubation time t (**b**).

Figure 8 displays the *M–H* curves of the $(Fe_{0.4}Co_{0.6})_{79}Nb_3B_{18}$ alloys annealed at 764 K, 800 K, 880 K, 974 K, and 1151 K for 90 s, respectively. The insert clearly shows the relationship between M_s

and H_c and annealing temperature. The VSM results indicate that the saturation magnetization (M_s) increases first and then decreases with the increase of annealing temperature. The alloys annealed at 880 K exhibit the optimized soft magnetic properties with high M_s of 145 emu g^{-1} and low H_c of 0.04 Oe. The α-(Fe, Co) and Fe$_{23}$B$_6$ phases are ferromagnetic [17,23], while Fe$_2$B or Fe$_3$B phases belong to the hard magnetic phase [14]. During the annealing process, more and more short-range ordered clusters are formed within the amorphous matrix, and the coupling of these clusters leads to anisotropy. With the increase of annealing temperatures ranging from 764 K to 880 K, the crystallization products remain the same, while the mean grain size decreases. The ferromagnetic exchange between these α-Fe(Co) nanocrystals is enhanced, thus leading to an increase of M_s. However, further increase of the annealing temperature results in coarse crystals with the precipitation of hard magnetic phases Fe$_2$B or Fe$_3$B [24,25]. As a result, the M_s value of the alloys is found to decrease.
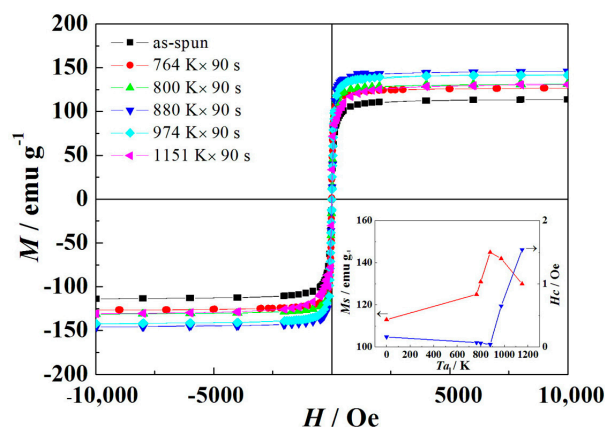

Figure 8. Room-temperature magnetization hysteresis curves for the (Fe$_{0.4}$Co$_{0.6}$)$_{79}$Nb$_3$B$_{18}$ alloys annealed at different temperatures.

According to the random anisotropy model (RAM) proposed by Hezer [26], the coercivity H_c is expressed as follows:

$$H_c \approx p_c \frac{K_1{}^4 D^6}{J_s A^3}, \tag{5}$$

where p_c is the dimensionless pre-factor of the order of unity, K_1 is the magneto-crystalline anisotropy, A is exchange stiffness, and J_s is saturation polarization.

The coercivity of the annealed (Fe$_{0.4}$Co$_{0.6}$)$_{79}$Nb$_3$B$_{18}$ alloys is quite low. Similar results were also obtained in the Fe$_{74}$Cu$_{0.8}$Nb$_{2.7}$Si$_{15.5}$B$_7$ alloys reported by Hoque et al. [27]. The coercivity of the annealed (Fe$_{0.4}$Co$_{0.6}$)$_{79}$Nb$_3$B$_{18}$ alloys decreases first and then increases with the increase of annealing temperature. With the increase of annealing temperatures in the range of 764–880 K, the crystallization products remain the same, and mean grain size decreases, leading to a decrease of H_c value. However, a further increase of annealing temperature results in the formation of the Fe$_2$B or Fe$_3$B phases. It is reported that the K_1 values for the Fe$_2$B or Fe$_3$B phases are equal to 430 kJ/m^3 [24,27], which are larger than that of the α-Fe(Co) phase. Therefore, this increase would significantly increase the magneto-crystalline anisotropy, thus leading to an increase of H_c value.

4. Conclusions

(1)　During the crystallization process in the (Fe$_{0.4}$Co$_{0.6}$)$_{79}$Nb$_3$B$_{18}$ alloys, a mixture of α-Fe(Co), Fe$_2$B, and Fe$_{23}$B$_6$ phases is first precipitated from the amorphous matrix, and then the formation of α-Fe(Co), Fe$_2$B, and Fe$_3$B phases occurs due to the decomposition of the metastable Fe$_{23}$B$_6$ phase.

(2)　For alloys annealed at $T_g \sim T_{x1}$, as the incubation time increases, the saturation magnetization first remains unchanged, and then increases steadily, while the coercivity decreases first and then increases.

(3) The mean grain sizes of the annealed $(Fe_{0.4}Co_{0.6})_{79}Nb_3B_{18}$ alloys first decrease and then increase with the increase of annealing temperature. The mean grain size reaches the minimum value of 12.7 nm for alloys annealed at 880 K.

(4) The annealed $(Fe_{0.4}Co_{0.6})_{79}Nb_3B_{18}$ alloys exhibit excellent magnetic properties with high saturation magnetization and low coercivity. With the increase of annealing temperature, the saturation magnetization first increases and then decreases, while coercivity is not obviously enhanced. The alloys annealed at 880 K with the finest grain size exhibit the optimized soft magnetic properties.

References

1. Yoshizawa, Y.; Oguma, S.; Yamauchi, K. New Fe-based soft magnetic alloys composed of ultrafine grain structure. *J. Appl. Phys.* **1988**, *64*, 6044–6066. [CrossRef]

2. Rizal, C.; Kolthammer, J.; Pokharel, R.K.; Choi, B.C. Magnetic properties of nanostructured Fe-Co alloys. *J. Appl. Phys.* **2013**, *113*, 113905. [CrossRef]

3. Inoue, A.; Shen, B.L.; Koshiba, H.; Kato, H.; Yavari, A.R. Cobalt-based bulk glassy alloy with ultrahigh strength and soft magnetic properties. *Nat. Mater.* **2003**, *2*, 661–663. [CrossRef] [PubMed]

4. Willard, M.A.; Laughlin, D.E.; McHenry, M.E.; Thoma, D.; Sickafus, K.; Cross, J.O.; Harris, V.G. Structure and magnetic properties of $(Fe_{0.5}Co_{0.5})_{88}Zr_7B_4Cu_1$ nanocrystalline alloys. *J. Appl. Phys.* **1998**, *84*, 6773–6777. [CrossRef]

5. McHenry, M.E.; Willard, M.A.; Laughlin, D.E. Amorphous and nanocrystalline materials for applications as soft magnets. *Prog. Mater. Sci.* **1999**, *44*, 291–433. [CrossRef]

6. Tang, J.C.; Mao, X.Y.; Li, S.D.; Gao, W.L.; Du, Y.W. Effects of two-step annealing on the microstructures and soft magnetic properties of nanocrystalline $Fe_{86}Zr_7B_6Cu_1$ ribbons. *J. Alloys Compd.* **2004**, *375*, 233–238. [CrossRef]

7. Cao, C.C.; Fan, J.W.; Zhu, L.; Meng, Y.; Wang, Y.G. Effects of relaxation time on local structural and magnetic properties of $Fe_{80.8}B_{10}P_8Cu_{1.2}$ amorphous alloy. *Acta Phys. Sin.* **2017**, *66*, 167501. (In Chinese)

8. Fan, X.D.; Zhang, T.; Jiang, M.F.; Yangc, W.M.; Shen, B.L. Synthesis of novel FeSiBPCCu alloys with high amorphous forming ability and good soft magnetic properties. *J. Non-Cryst. Solids* **2018**, in press. [CrossRef]

9. Parsons, R.; Zang, B.; Onodera, K.; Kishimoto, H.; Kato, A.; Suzuki, K. Soft magnetic properties of rapidly-annealed nanocrystalline Fe-Nb-B-(Cu) alloys. *J. Alloys Compd.* **2017**, *723*, 408–417. [CrossRef]

10. Xue, L.; Yang, W.M.; Liu, H.S.; Men, H.; Wang, A.; Chang, C.T.; Shen, B.L. Effect of Co addition on the magnetic properties and microstructure of FeNbBCu nanocrystalline alloys. *J. Magn. Magn. Mater.* **2016**, *419*, 198–201. [CrossRef]

11. Ramanujan, R.V.; Zhang, Y.R. Quantitative transmission electron microscopy analysis of the nanocrystallization kinetics of soft magnetic alloys. *Phys. Rev. B* **2006**, *74*, 224408. [CrossRef]

12. Kotan, H.; Darling, K.A.; Saber, M.; Scattergood, R.O.; Koch, C.C. An in situ experimental study of grain growth in a nanocrystalline $Fe_{91}Ni_8Zr_1$ alloy. *J. Mater. Sci.* **2013**, *48*, 2251–2257. [CrossRef]

13. Sahoo, T.; Majumdar, B.; Srinivas, V.; Srinivas, M.; Nath, T.K.; Agarwal, G. Improved magnetoimpedance and mechanical properties on nanocrystallization of amorphous $Fe_{68.5}Si_{18.5}Cu_1Nb_3B_9$ ribbons. *J. Magn. Magn. Mater.* **2013**, *343*, 13–20. [CrossRef]

14. Xue, L.; Liu, H.S.; Dou, L.T.; Yang, W.M.; Chang, C.T.; Inoue, A.; Wang, X.M.; Li, R.W.; Shen, B.L. Soft magnetic properties and microstructure of $Fe_{84-x}Nb_2B_{14}Cu_x$ nanocrystalline alloys. *Mater. Design* **2014**, *56*, 227–231. [CrossRef]

15. Li, P.; Su, H.L.; Song, Y.J.; Wu, Y.C. Effects of annealing temperature on microstructure and magnetic properties of $Fe_{73.37}Cu_{0.92}Nb_{2.9}Si_{13.56}B_{9.24}$ amorphous alloy. *Mater. Sci. Technol.* **2013**, *29*, 460–463. [CrossRef]

16. Jiang, J.Z. Anomalous grain growth in nanocrystalline $Fe_{73.5}Cu_1Nb_3Si_{13.5}B_9$ alloys. *Nanostruct. Mater.* **1997**, *9*, 245–248. [CrossRef]

17. Stoica, M.; Kumar, S.; Roth, S.; Ram, S.; Eckert, J.; Vaughan, G.; Yavari, A.R. Crystallization kinetics and magnetic properties of $Fe_{66}Nb_4B_{30}$ bulk metallic glass. *J Alloys Compd.* **2009**, *483*, 632–637. [CrossRef]

18. Torrens-Serra, J.; Rodríguez-Viejo, J.; Clavaguera-Mora, M.T. Nanocrystallization kinetics and glass forming ability of the $Fe_{65}Nb_{10}B_{25}$ metallic alloy. *Phys. Rev. B* **2007**, *76*, 214111. [CrossRef]

19. Imafuku, M.; Sato, S.; Koshiba, H.; Matsubara, E.; Inoue, A. Crystallization behavior of amorphous $Fe_{90-X}Nb_{10}B_X$ (X = 10 and 30) alloys. *Mater. Trans. JIM* **2000**, *41*, 1526–1529. [CrossRef]

20. Yao, B.; Guo, H.C.; Wang, J.; Ding, B.Z.; Li, H.; Wang, A.M.; Hu, Z.Q. Influence of pressure on the grain sizes in the crystallization process of an amorphous Fe-Mo-Si-B alloy. *Phys. B Condens. Matter* **1996**, *228*, 379–382. [CrossRef]

21. Yang, W.M.; Liu, H.S.; Dun, C.C.; Zhao, Y.C.; Dou, L.M. The mechanism of the anomalous variation of grain size for Fe-based nanocrystalline alloys. *Acta Phys. Sin.* **2012**, *61*, 106802. (In Chinese)

22. Guo, Y.C.; Wang, Z.X. *Amorphous State Physics*, 1st ed.; Scientific Press: Beijing, China, 1984; pp. 129–145. (In Chinese)

23. Shen, B.L.; Men, H.; Inoue, A. Fe-based bulk glassy alloy composite containing in situ formed *á*-(Fe, Co) and $(Fe, Co)_{23}B_6$ microcrystalline grains. *Appl. Phys. Lett.* **2006**, *89*, 101915. [CrossRef]

24. Gao, J.E.; Li, H.X.; Jiao, Z.B.; Wu, Y.; Chen, Y.H.; Yu, T.; Lu, Z.P. Effects of nanocrystal formation on the soft magnetic properties of Fe-based bulk metallic glasses. *Appl. Phys. Lett.* **2011**, *99*, 052504. [CrossRef]

25. Zhu, M.; Fa, Y.; Jian, Z.Y.; Yao, L.J.; Jin, C.Q.; Nan, R.H.; Chang, F.E. Non-isothermal crystallization kinetics and soft magnetic properties of the $Fe_{67}Nb_5B_{28}$ metallic glasses. *J. Therm. Anal. Calorim.* **2018**, *132*, 173–180. [CrossRef]

26. Hezer, G. Grain size dependence of coercivity and permeability in nanocrystalline ferromagnets. *IEEE Trans. Magn.* **1990**, *26*, 1397–1402. [CrossRef]

27. Hoque, M.S.; Hakim, M.A.; Dhar, U.; Saha, D.K.; Nordblad, P.; Paul, D.P. Detailed study of ultra-soft magnetic properties of $Fe_{74}Cu_{0.8}Nb_{2.7}Si_{15.5}B_7$. *Philos. Mag.* **2011**, *91*, 2117–2139. [CrossRef]